ASCE

Regional Seismic Risk Assessment of Infrastructure Systems through Machine Learning: Active Learning Approach

Sujith Mangalathu, Ph.D., A.M.ASCE[1]; and Jong-Su Jeon, Ph.D.[2]

Abstract: Regional seismic risk assessment involves many infrastructure systems, and it is computationally intensive to conduct an individual simulation of each system. This paper suggests an approach using active learning to select informative samples that help build machine learning models with fewer samples for regional damage assessment. The potential of the approach is demonstrated with (1) failure mode prediction of bridge columns, and (2) regional damage assessment of the California two-span bridge inventory with seat abutments. The active learning approach involves the selection of column attributes or bridge models that are more informative to the creation of machine learning-based decision boundaries. The results reveal that an active learning target model based on 100 bridge samples can achieve a level of accuracy of 80%, which is equivalent to a machine learning model based on 480 bridge samples in the case of damage prediction following an earthquake. With the proposed approach, the computational complexity associated with regional risk assessment of bridge systems with specific attributes can be drastically reduced. The proposed approach also will help plan experimental studies that are more informative for damage assessment. **DOI: 10.1061/(ASCE)ST.1943-541X.0002831.**

Author keywords: Machine learning; Active learning; Column failure mode; Bridge tagging; Regional seismic risk.

Introduction

Regional risk assessment of infrastructure systems is an active research topic in earthquake engineering and infrastructure resilience (Mangalathu et al. 2017; Silva et al. 2014; Mangalathu and Burton 2019; Morfidis and Kostinakis 2018; Argyroudis et al. 2019), as a proper regional assessment leads to informed recovery and resilience strategies in a postearthquake scenario. The time required to recover some fraction of predisaster infrastructure functionality and viable options to improve performance are of prime importance after a natural hazard event. The recovery efforts can be optimized by a proper regional risk assessment of infrastructure systems. However, the spatial distribution of the infrastructure systems together with specific geometric, material, and structural properties leads to a challenge in assessing the risk and vulnerability of infrastructure systems. To give an example, the highway network in California consists of more than 24,000 bridges, for which it is very time-consuming and expensive to obtain the structure-specific properties (Mangalathu 2017). Note that the structure-specific properties include the geometric properties of the bridge, associated material properties, configurations and layout of bridges (e.g., skew, curve, balance), and soil properties. The strategy that is traditionally adopted is to sample the bridges randomly and estimate the properties of individual bridge attributes either through visual inspection or plan review using statistical techniques (Mangalathu et al. 2016). The bridge samples generated using these statistical properties are used to estimate the risk and vulnerability of bridge stocks. Although these approaches provide useful insights and information, they are not useful for bridge-specific damage identification (Mangalathu and Jeon 2019b).

The need for bridge-specific risk assessment has led to a considerable number of studies in this research direction (Seo et al. 2012; Seo and Linzell 2013; Shekhar and Ghosh 2020; Dukes et al. 2018; Mangalathu et al. 2018a, b; Mangalathu and Jeon 2019b). These approaches involve estimating the seismic demand model as a function of bridge attributes using machine learning or response surface methods. The estimated demand model is then convolved with precomputed capacity models, and machine learning methods are used to obtain bridge-specific vulnerability values. However, these approaches require considerable amounts of data to establish the seismic demand model, and the data often are obtained through extensive numerical computations. These extensive data requirements can be bypassed through the selection of informative samples through an approach called active learning. Active learning aims to increase the efficiency and economics of a machine learning model through the acquisition of limited samples and associated outputs. Although active learning is an attractive theme in the field of machine learning (Settles 2010; Cohn et al. 1996; Konyushkova et al. 2017), this technique has not been explored in the field of seismic regional risk assessment. Most machine learning studies in earthquake engineering have been limited to failure mode or damage estimation through data collected from experimental or numerical studies (Kiani et al. 2019; Siam et al. 2019; Huang and Burton 2019; Mangalathu and Jeon 2018, 2019a; Mangalathu et al. 2019; Mangalathu and Burton 2019).

Addressing the extensive data requirement, which is either computationally expensive or not available in many scenarios in earthquake engineering, this study (1) explores the feasibility of active learning approaches for damage assessment of infrastructure systems, (2) compares the various active learning approaches (i.e., whether samples should be queried one by one or in groups),

[1]Research Data Scientist, Mangalathu, Puthoor PO, Kollam, Kerala 691507, India. Email: sujithmss@gatech.edu

[2]Assistant Professor, Dept. of Civil and Environmental Engineering, Hanyang Univ., Seoul 04763, Republic of Korea (corresponding author). ORCID: https://orcid.org/0000-0001-6657-7265. Email: jongsujeon@hanyang.ac.kr

Note. This manuscript was submitted on March 4, 2020; approved on June 16, 2020; published online on September 22, 2020. Discussion period open until February 22, 2021; separate discussions must be submitted for individual papers. This paper is part of the ***Journal of Structural Engineering***, © ASCE, ISSN 0733-9445.

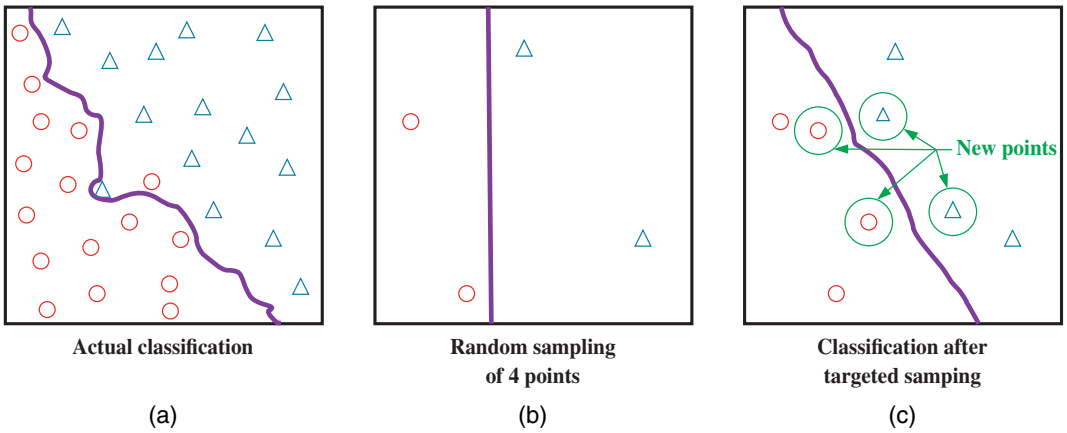

Fig. 1. Demonstration of active learning approach: (a) actual decision boundary; (b) decision boundary based on four random samples; and (c) improved decision boundary based on four random samples and four targeted samples.

(3) suggests an approach to plan experimental studies that are more informative in the creation of machine learning models for damage identification, and (4) proposes a computationally less expensive procedure for damage assessment of infrastructure systems at a regional scale. The appropriateness of the proposed approach is demonstrated in two ways: (1) failure mode prediction of bridge columns, and (2) damage assessment of California bridge systems. In the former, experimental results are used, while the latter uses the results from nonlinear dynamic simulations of bridge systems. This study selects the bridge columns as one of the case studies because the availability of their experimental data is higher than other bridge components. The intuition behind the selection of two-span bridges is that (1) this bridge class occupies the largest portion of the California bridge inventory, and (2) has been used as the subject structure of extensive studies (e.g., Ramanathan 2012; Mangalathu et al. 2019). The results of the current study reveal the potential of active learning approaches for regional damage analysis with less data.

Active Learning Approaches

Active learning is a branch of machine learning that can overcome the large labeling requirement by using queries in the form of unlabeled instances to be labeled. Labeling can be performed with the help of an engineer based on his/her experience or insights from experimental observations and numerical simulations. The active learning approach can build a better machine learning model with minimal labels. For example, in the case of the bridge tagging with numerical simulations, extensive computational effort and time are required to obtain labels through numerical simulation. The active learning approach consists of initially selecting a minimal number of samples and obtaining the corresponding labels or classes to which they belong. A machine learning model is established based on these data, and an active learner selects targeted samples to improve the model. The new samples are added to the original data, and the model is reconstructed. Fig. 1 shows an illustration of the active learning approach for a two-classification problem, and Fig. 1(a) shows the actual decision boundary when the labels are available for the entire database. Four samples are randomly selected, and a machine learning model is initially established (four are arbitrarily chosen to demonstrate the concept) [Fig. 1(b)]. The initial decision boundary (shown as a solid line) varies depending on the machine learning model and is shown as a vertical line to illustrate the concept. The active learner selects four new samples close to the current classification model and obtains the corresponding labels [Fig. 1(c)]. A new machine learning model is established with the initial and new data, and the new decision boundary improves the current classification model. For the data shown in Fig. 1, the new decision boundary with eight samples (four random samples and four targeted samples) well matches the actual classification model. The current classification model can be improved further with additional targeted samples. Two active learning approaches, pool-based sampling and ranked batch mode sampling, are used in this study and are explained in the following sections.

Pool-Based Sampling

Pool-based sampling assumes that there is a larger amount of unlabeled data available and that the data do not change over time. These assumptions hold true in this study as the input and output properties in selected cases (here, column failure modes, and bridge tags) are stationary. For a random variable $X = (X_1, \ldots, X_n)$ with associated class labels Y, assume that labels are known for a small data set, $L = (x_i, y_i)$, and that a large unknown data set $U = (x_i, y_i)$ is available. Note that x and y represent specific instances of X and Y, respectively. The most informative target sample $(x^*, ?)$ is obtained in pool-based sampling based on its utility (e.g., reduction in classification error). The algorithm for pool-based sampling for the regional risk assessment problem is provided in Algorithm 1.

Algorithm 1. Algorithm for uncertainty pool-based sampling

1. Input (U–unlabeled data, L–labeled data, M–machine learning model, C–computational limitation or experimental limitation)
2. Repeat until C
   for all $(x^*, ?) \in U$, compute the utility of x^* and pick the one with the highest value
   update $L \leftarrow L \cup (x^*, y^*)$
   $U \leftarrow U \setminus (x^*, y^*)$

The widely used uncertainty sampling approach is used in this study (Settles 2010). For a two-class classification problem, uncertainty sampling queries targeted samples with a probability close to 0.5 (Lewis and Catlett 1994). In general, target samples are those

close to the current decision boundary model. The utility measure adopted in the current study is classification entropy (H)

$$H(x) = -\sum_k p_k \log(p_k) \quad (1)$$

where p_k = probability that x^* belongs to class k.

Batch Mode Sampling

Contrary to pool-based sampling, where samples are selected for labeling one at a time, a group of samples is selected for labeling in batch mode sampling. The individual pool-based sampling strategy fails in group-based sampling due to overlap between samples (Cardoso et al. 2017). Many strategies have been developed to alleviate this limitation, and one of the common approaches is ranked batch mode sampling. In ranked batch mode sampling, the model developed using L is used to estimate the confidence of the classification and its uncertainty score ($U_{\text{uncertainty}}$). This information is used to rank the unlabeled data, U, and the selected sampling group (Q) is passed for labels. The algorithm of the process is explained in detail in Algorithm 2 and discussed in depth in Cardoso et al. (2017). The uncertainty score is estimated as $1 - p_k$, as the focus is on minimizing the classification error, and ranking is based on the similarity index (Cardoso et al. 2017).

Algorithm 2. Algorithm for ranked batch mode sampling

1. Input (U–unlabeled data, L–labeled data, M–machine learning model, C–computational limitation or experimental limitation, Q–group for labels)
2. $U_{\text{uncertainty}} = \text{uncertainty estimation}\,(U, L)$
   $L_{\text{estimated}} = L$, ranked instances
3. Repeat until C
   for all $(x^*, ?) \in U$
   $s = \text{select instance}\,(L_{\text{estimated}}, U_{\text{uncertainty}})$
   $L_{\text{estimated}} \leftarrow L_{\text{estimated}} \cup s$
   $U_{\text{uncertainty}} \leftarrow U_{\text{uncertainty}} / s$
   updatelist Q with s
   update $L \leftarrow L \cup Q$
   $U \leftarrow U \setminus Q$

Active Learning Approaches for Damage Assessment

To demonstrate the concept of active learning for damage assessment of infrastructure systems, two tasks are carried out: (1) failure mode identification of bridge columns, and (2) damage assignment of bridge inventory. In the first task, this study uses experimental results summarized in Mangalathu and Jeon (2019a). It is often expensive to carry out experimental studies, and the objective of the first task is to demonstrate that a good machine learning model for failure mode prediction can be obtained with fewer data. In the second task, damage-state machine learning models are established for two-span seat abutment bridges with a two-column bent in California. The details of these tasks are described in the following section.

Column Failure Mode Identification

Mangalathu and Jeon (2019a) assembled 311 experimental circular column specimens that would fail in either flexure (F), shear (S), or combined mode (flexure-shear, FS). Based on exploratory data analysis, the authors identified four input variables: aspect ratio, axial load ratio, and longitudinal and transverse reinforcement

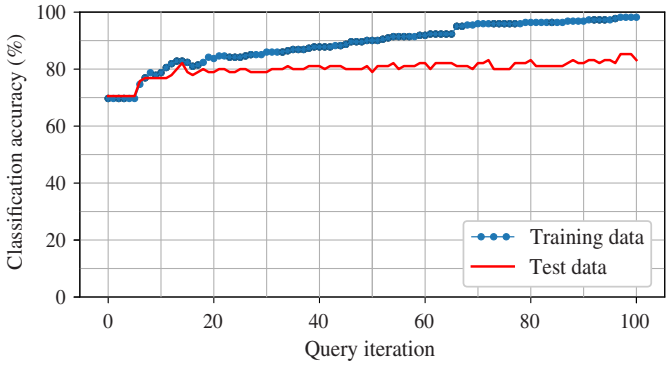

Fig. 2. Incremental classification accuracy for column failure mode using pool-based sampling.

indices. A detailed analysis of the input variables, machine learning models, and associated inferences are presented in Mangalathu and Jeon (2019a). Two active learning approaches, pool-based sampling and ranked batch mode sampling, are explored to obtain a machine learning model with fewer input parameters. Out of 311 samples, 70% are used as the training set, and the remaining data serve as the test set. Keeping a portion of data as the test set helps evaluate the performance of the model on the unknown data. In pool-based sampling, samples are queried one after another. Fig. 2 shows the variation in total accuracy with the query iteration. An initial machine model is established using XGBoost (Chen and Guestrin 2016) with 10 randomly selected samples. A detailed comparison of the various machine learning models can be found in Mangalathu and Jeon (2019a). The model will work for any machine learning model under consideration, and XGBoost is adopted in this study as it is one of the most widely used machine learning models (Chen and Guestrin 2016). The XGBoost training parameters include 100 boosting stages, a subsampling rate of 1.0, the mean squared error with improvement score by Friedman (2001) to split the trees with a minimal split of two samples, and a learning rate of 0.1 (Mangalathu et al. 2020). As noted in Mangalathu et al. (2020), the gradient boosting is robust to overfitting and the selected parameters deemed sufficient. The parameters are kept constant in the active learning iterations for a fair comparison. Fig. 2 shows that the subsequent pool-based queries show increased performance after each iteration. Although a limit of 100 queries is set in this study, the actual number of queries depends on external factors such as budget constraints and simulation limitations. In a real scenario, the model only selects the input parameters that can increase its performance, and the user must plan further experimental studies for that scenario. The current study relies on the available input parameters and the corresponding failure modes. Here, accuracy is the ratio of predictions that are correctly predicted by the machine learning algorithm. The accuracy of the training set and the test set increases with each iteration, as evident in Fig. 2.

The performance of the model can be explored in detail with the help of a confusion matrix, which is a table of actual versus estimated predictions. The confusion matrix provides more insight into not only the performance of the machine learning based failure mode prediction model but also which failure modes are being predicted correctly, in the form of precision and recall. Fig. 3 shows the confusion matrix of the training set and test set after 50 and 100 iterations along with the associated precision and recall for failure modes: flexure (F), flexure-shear (FS), and shear (S). Precision identifies the percentage of correct predictions, whereas recall identifies which portions are correctly identified. The confusion matrix

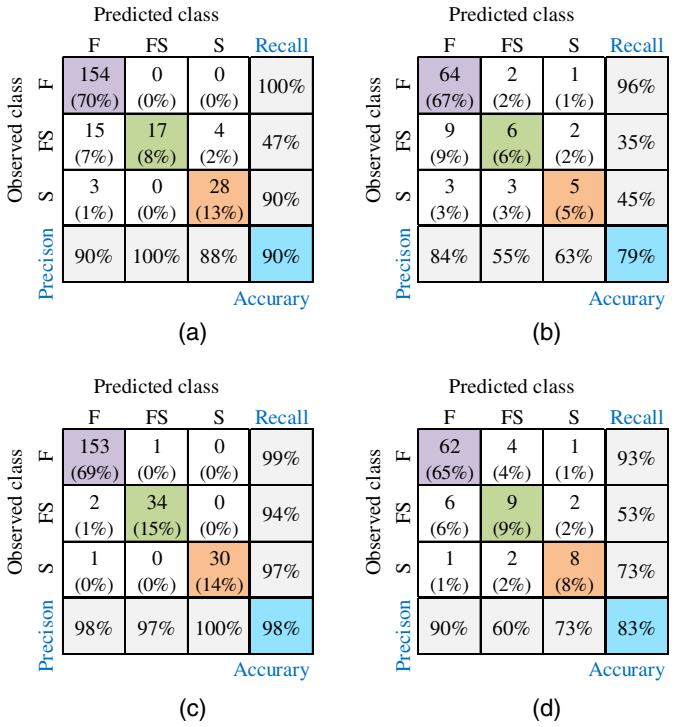

Fig. 3. Confusion matrix for column failure mode using pool-based sampling: (a) after 50 iterations (training set); (b) after 50 iterations (test set); (c) after 100 iterations (training set); and (d) after 100 iterations (test set).

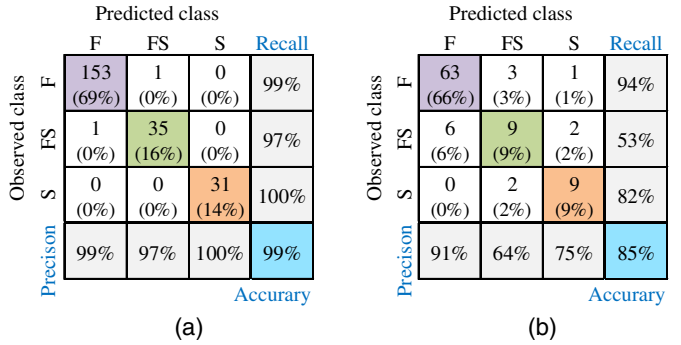

Fig. 4. Confusion matrix for the entire dataset of column failure mode: (a) with the training set; and (b) with the test set.

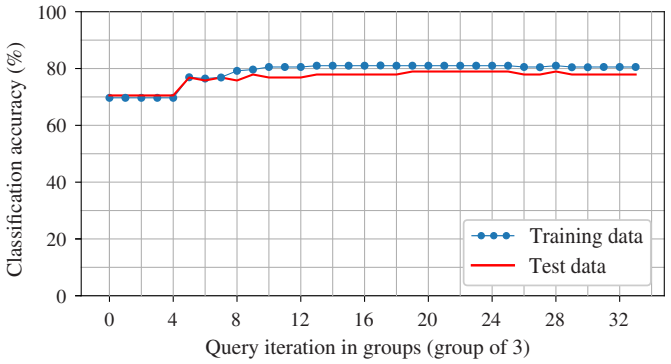

Fig. 5. Incremental classification accuracy for column failure mode using ranked batch mode sampling.

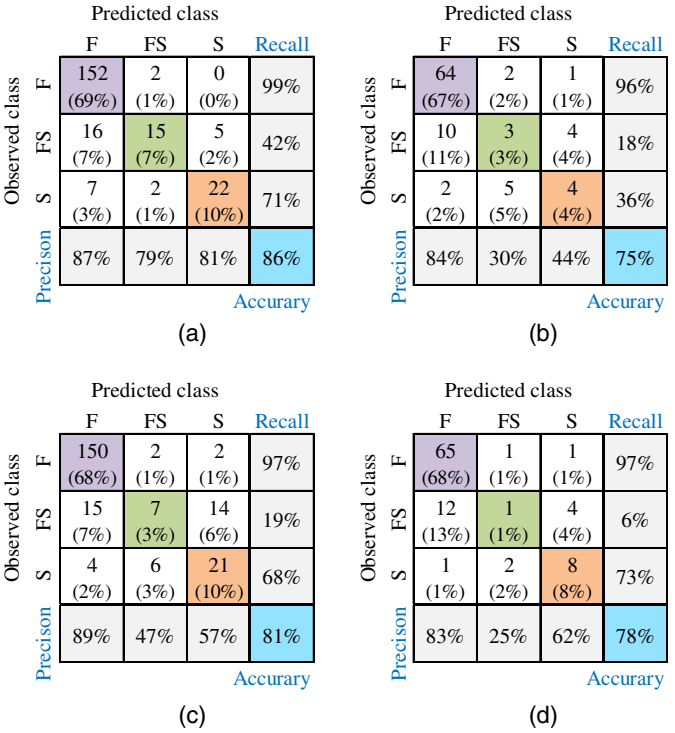

Fig. 6. Confusion matrix for column failure mode using ranked batch model sampling: (a) after 50 iterations (training set); (b) after 50 iterations (test set); (c) after 100 iterations (training set); and (d) after 100 iterations (test set).

after 50 iterations represents that only 50 samples are used in addition to the original 10 samples to establish the machine learning model, while 100 samples indicate the use of 110 samples (100 selected samples and 10 original samples). The addition of more data enhances the performance of the model, and the classification accuracy after 100 iterations is higher than 50 iterations, as expected (Fig. 3). Fig. 4 depicts the confusion matrix using the entire dataset, which can be regarded as the upper bound of accuracy possible with the given data. The model can reach a relative accuracy of 92% (ratio of 0.79 to 0.85) for the training set after 50 iterations, and the relative accuracy increases to 97% after 100 iterations. The attainment of 97% relative accuracy with 100 samples is an indication of the power of the method for obtaining a good prediction model with a relatively small number of samples.

Fig. 5 shows the plot of classification accuracy (in percentile) versus the number of queries. Like pool-based sampling, the initial model is built with the same 10 random samples. As the samples are passed in groups for ranked batch mode sampling, a group of three samples is chosen, and the maximum queries are limited to 100 (~33 group queries). Contrary to pool-based sampling (Fig. 2), the accuracy does not change much with iterations (for both the training set and the test set) after 12 group queries, which also is evident from the confusion matrix tables (Fig. 6). The accuracy after 100 iterations for the training set is only 78% for ranked batch mode sampling, while it is 85% for pool-based sampling.

To compare the advantage of active learning compared to random sampling, analyses are carried out with random samples.

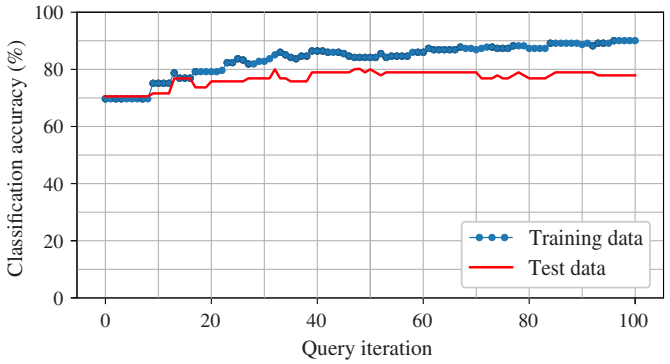

Fig. 7. Incremental classification accuracy for column failure mode using random sampling.

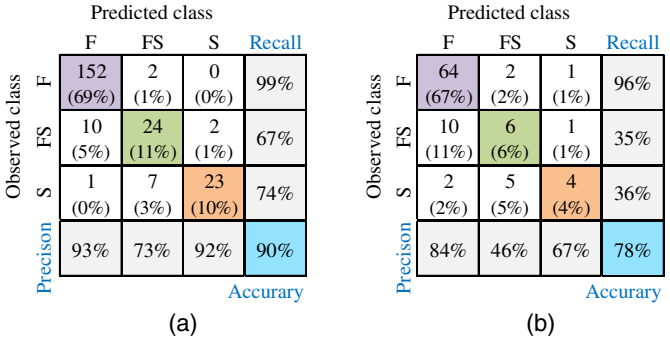

Fig. 8. Confusion matrix for column failure mode using random sampling: (a) after 100 iterations (training set); and (b) after 100 iterations (test set).

In this approach, the data are randomly selected, and models are updated based on the additional information from the random samples. For a random sampling approach, the total accuracy after 100 iterations for the training set and the test set is 90% and 78%, respectively, as shown in Fig. 7. In contrast, for the pool-based approach, the total accuracy after 100 iterations for the training set and the test set is 98% and 83%, respectively (Fig. 3). In addition, the confusion matrix of the random learning approach with 100 iterations is presented in Fig. 8, and it refers to the precision and recall of the model for various failure modes. The comparison of Figs. 3 and 8 indicates that the active learning approach performs better compared to the random sampling approach.

The active learning results on experimental column data indicate the potential of the approach for cases such as regional risk assessment where (1) the experimental data are often rare or limited, and (2) extensive computational approaches are needed to create data. The latter is explored in the next section.

Damage Assessment of Bridge Inventory at Regional Scale

The insights from the observations in the previous section are used to create a procedure for regional-scale damage estimation of bridges following an earthquake. It is critical to understand the failure of bridges for efficient recovery, loss estimation, and resilience measures. However, each bridge has its own soil conditions and geometric, structural, and material properties; these unique

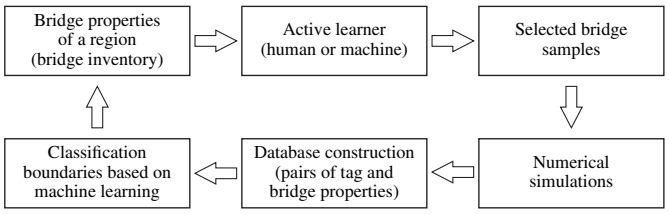

Fig. 9. Damage assessment of bridges using the active learning approach.

attributes demand numerical modeling of each bridge for efficient damage estimation. As regional-scale experimental data are scarce, numerical simulation results are used for damage assessment, generating a huge computational demand. The suggested procedure for damage assessment of bridges without a huge computational onus is provided in Fig. 9. The procedure is iterative and involves (1) assembling the bridge-specific properties in a region and creating numerical modeling of some random samples, (2) estimating the damage state of the bridge and training a machine learning model based on the initial data, (3) employing an active learning strategy to query the most informative bridge samples, (4) creating numerical modeling of the queried samples and estimating the damage, and (5) revising the machine learning model. The process can be terminated by the user based on computational onus or budget constraints. The proposed approach is demonstrated with two-span bridges that account for more than 40% of the bridge inventory in California. Following the work of Mangalathu et al. (2019) with columns as the critical component of the bridges, three damage states are accounted for in this study: (1) no damage to the column (green state, G), (2) concrete spalling and yielding of longitudinal reinforcement (yellow state, Y), and (3) irreparable damage to the columns (red state, R). The numerical modeling methods of the bridge, ground motion selection, and bridge data are explained in detail in the following section.

Computational Modeling Assumptions of Subject Bridge and Ground Motion Selection

The numerical modeling of the selected two-span bridge is shown in Fig. 10. For this type of bridge, an expansion joint exists between the superstructure and abutment. Using the finite element program OpenSees (McKenna 2011), a three-dimensional computational model of the subject bridge is generated by assembling the responses of individual bridge components. The numerical model can account for geometric and material nonlinearities. As noted from past earthquakes, the superstructure remains elastic during seismic excitations and is thus modeled using elastic beam-column elements, while rigid elements are used to represent transverse beams and superstructure-column connections. Columns comprise nine displacement-based beam-column elements that can capture the inelastic behavior of columns. Translational and rotational zero-length elements are assigned at the center of footings to simulate the behavior of soil-structure interaction. The active response of the abutment is assumed to be the response of abutment piles, which are modeled by a trilinear material model from Mangalathu et al. (2016), and the abutment passive response is represented by the combined action of soil backfill and piles. The response of the backfill is simulated using the hyperbolic model of Shamsabadi et al. (2010). The expansion joint includes elastomeric bearings, external shear keys, and pounding between the deck and abutment. All spring elements in the expansion joint are located at bearing locations. The elastomeric bearings are used to offer longitudinal and transverse seismic resistance with respect to the bridge axis,

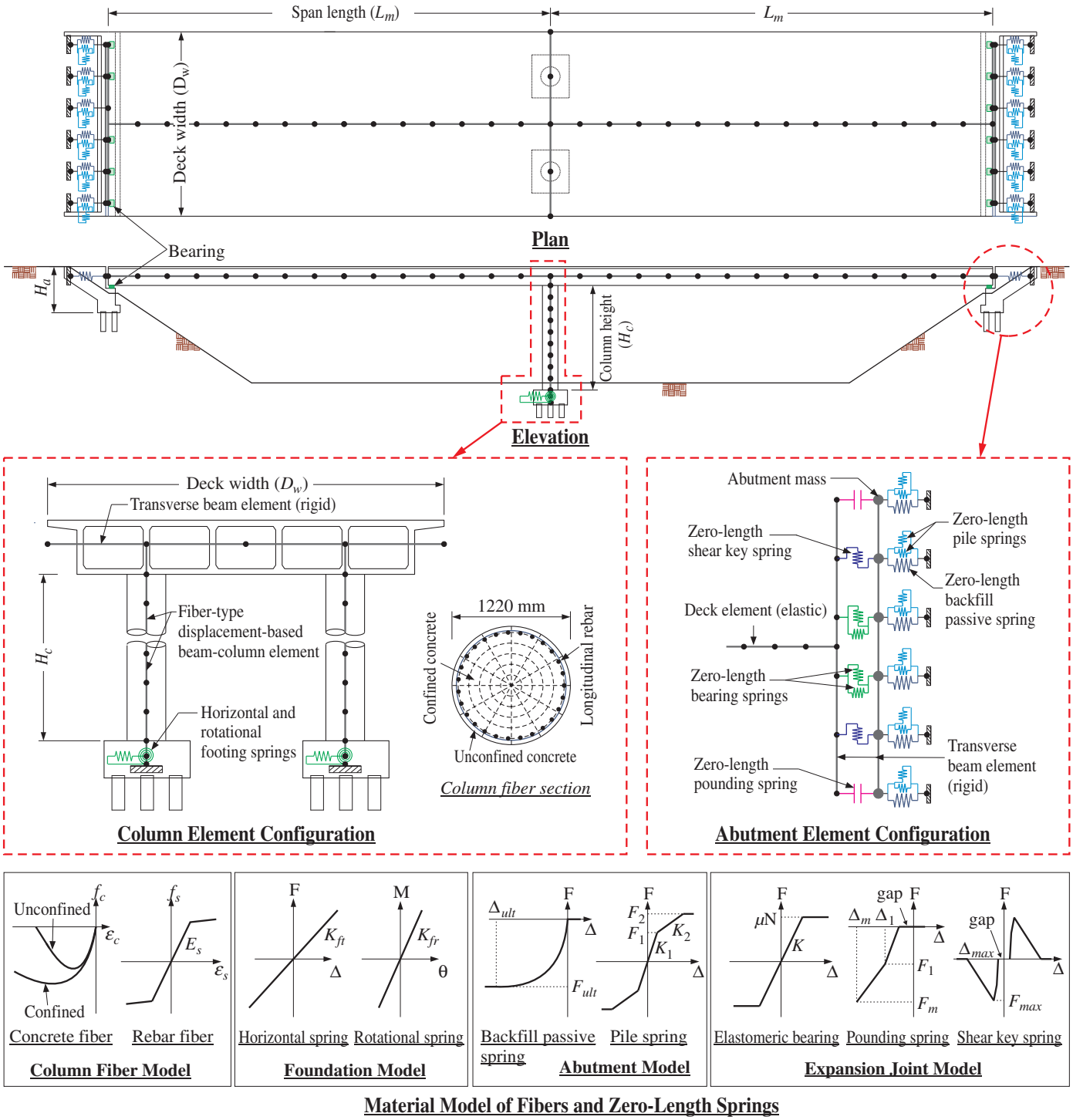

Fig. 10. Computational model of individual bridge components.

which can be idealized by a bilinear material model without hardening (Mangalathu et al. 2016). The pounding element is characterized as a zero-length element using the material model of Muthukumar and DesRoches (2006), which has inelastic compression-only behavior with a gap. The nonlinear response of shear keys, which are employed to prohibit lateral movement of the superstructure, is modeled using a trilinear material model with a gap. The material model is constructed following the experimental work of Silva et al. (2009). Rayleigh damping in the first two modes is considered in nonlinear dynamic simulations. Detailed descriptions of the computational modeling assumptions are provided in the references (Mangalathu et al. 2017; Mangalathu 2017).

The current study adopts the ground motion set constructed by Baker et al. (2011), which was generated to perform seismic risk assessment of infrastructure systems in California. This set comprises four subsets, and each of which has 40 pairs of ground motions (a total of 160 pairs). This study scales 160 horizontal ground motion pairs by factors of 1.5 and 2 to reflect higher probabilistic design hazard levels in California (Jeon et al. 2019). Thus, a total of 480 horizontal ground motion pairs is used in this research.

Table 1. Bridge attributes and their probability distribution

Parameter	Type	Parameters		Truncated limit	
		Mean	Standard deviation	Lower	Upper
Superstructure (prestressed concrete box-girder)					
Span length, L_m (m)	N	41.15	10.67	22.86	70.10
Width of the deck (five-cell deck), D_w (m)	N	17.37	2.44	15.24	20.12
Column					
Concrete compressive strength, f_c (MPa)	N	31.37	3.86	22.75	39.09
Rebar yield strength, f_y (MPa)	N	475.7	37.9	399.9	551.6
Clear height, H_c (m)	LN	7.13	1.15	5.18	9.75
Longitudinal reinforcement ratio, ρ_l	U	0.02	0.006	0.01	0.03
Transverse reinforcement ratio, ρ_t	U	0.009	0.003	0.004	0.013
Pile foundation					
Translational stiffness, K_{ft} (kN/mm)	LN	175.1	0.44	70.05	437.8
Transverse rotational stiffness, K_{fr}(GN · m/rad)	LN	1.36	0.28	0.54	3.39
Transverse/longitudinal rotational stiffness ratio, k_r	LN	1.0	1.5	0.67	1.5
Abutment on piles					
Abutment backwall height, H_a (m)	LN	3.59	0.65	2.90	6.10
Pile stiffness, K_p (kN/mm)	LN	0.124	0.045	0.058	0.234
Backfill type, BT (sand versus clay)	B	—	—	—	—
Expansion joint					
Bearing stiffness per deck width, K_b (N/mm/mm)	LN	0.630	0.299	0.230	1.436
Coefficient of friction of bearing pad, μ_b	N	0.3	0.1	0.1	0.5
Longitudinal gap (pounding), Δ_l (mm)	LN	23.3	12.4	7.6	55.9
Transverse gap (shear key), Δ_t (mm)	U	19.1	11.0	0	38.1
Acceleration for shear key capacity, $a_{sk}(g)$	LN	1	0.2	0.8	1.2
Other parameters					
Mass factor, m_f	U	1.05	0.06	0.95	1.15
Damping ratio, ξ	N	0.045	0.0125	0.02	0.07
Earthquake direction (fault-normal versus parallel), ED	B	—	—	—	—

Source: Data from Mangalathu (2017).
Note: N = normal; LN = lognormal; U = uniform; and B = Bernoulli distribution.

Following Ramanathan (2012), the spectral acceleration at 1.0 s is regarded as the ground motion intensity measure (IM), which serves as one of the input variables in damage evaluation of bridges.

Selected Bridge Samples

Since this study aims to perform damage assessment of bridge portfolios, bridge design attributes must be considered. Table 1 describes the mean value, standard deviation, and assumed probability distribution of the selected bridge attributes, which are based on the California bridge inventory assembled by Mangalathu (2017).

Estimation of Seismic Demand and Structural Capacity for Bridge Tagging

The bridge attributes are sampled using the Latin hypercube sampling technique (Stein 1987) to create statistically significant yet nominally identical bridge models. Special care is taken to ensure that the sampled model corresponds to a real bridge in California based on the bridge inventory assembled by Mangalathu (2017). Each computational bridge model is paired randomly with one of the ground motions. Two horizontal motions of each earthquake are randomly assigned to the bridge longitudinal and transverse axes. For 480 bridge-ground motion pairs, a set of nonlinear dynamic simulations is performed to monitor outputs related to the engineering demand parameter of bridge components. Following Mangalathu et al. (2019), maximum column curvature ductility is used as the engineering demand parameter in this research. The current study is limited to 480 bridge samples in California, and analysis of the entire set of two-span bridges in California is beyond the scope of this research.

Moment-curvature analysis is carried out to estimate the column capacity, and the comparison of demand and capacity yields the damage states shown in Fig. 11. In the figure, ϕ_y is the yield curvature (obtained by second stiffness method); ϕ_{spall} is the curvature at concrete spalling (where extreme fiber stress for cover concrete approaches zero); and ϕ_u is the ultimate curvature (loss of column lateral and vertical load-carrying capacity). In this study, the yield and spalling curvature are regarded as damage state thresholds, as explained in detail in Mangalathu et al. (2019). Table 2 presents a summary of the damage states used in this study.

Results of the Active Learning Approach for Bridges

An initial machine learning model is estimated using XGBoost (with 10 randomly selected bridge samples and the associated damage states) for both the pool-based and rank-based active learning approaches. As mentioned before, further input data are estimated one by one for the pool-based approach, and three samples are

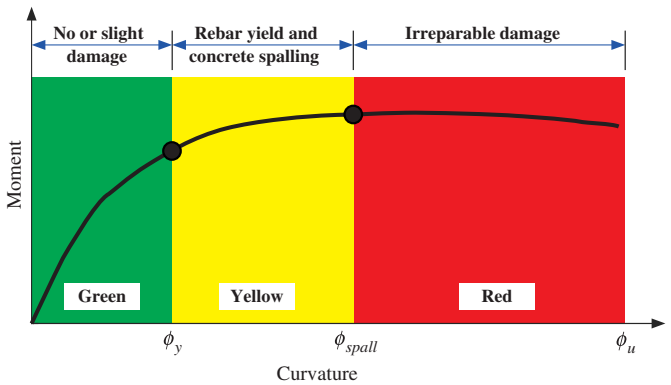

Fig. 11. Damage state threshold and the associated states of columns.

Table 2. Damage states of bridges and columns and implications on traffic

Damage states	Demand versus capacity	Column state	Column damage	Traffic implications
Green (G)	$\phi_d \le \phi_y$	None or aesthetic	EQ-related minor cracking	Open to normal public traffic—no restrictions
Yellow (Y)	$\phi_y \le \phi_d \le \phi_{spall}$	Minor or major repairs needed, but function intact	Minor spalling of cover concrete, exposed core, confinement yield	Emergency vehicles only—speed/weight/lane restrictions
Red (R)	$\phi_d \ge \phi_{spall}$	Irreparable damage, function compromised	Bar buckling, large drift, core crushing	Closed (until shored/braced)—potential for collapse

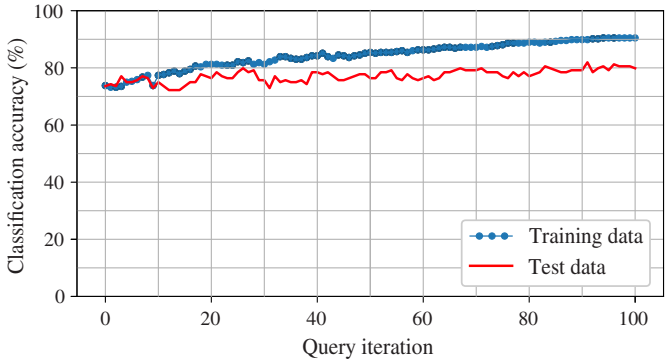

Fig. 12. Incremental classification accuracy for bridge damage state using pool-based sampling.

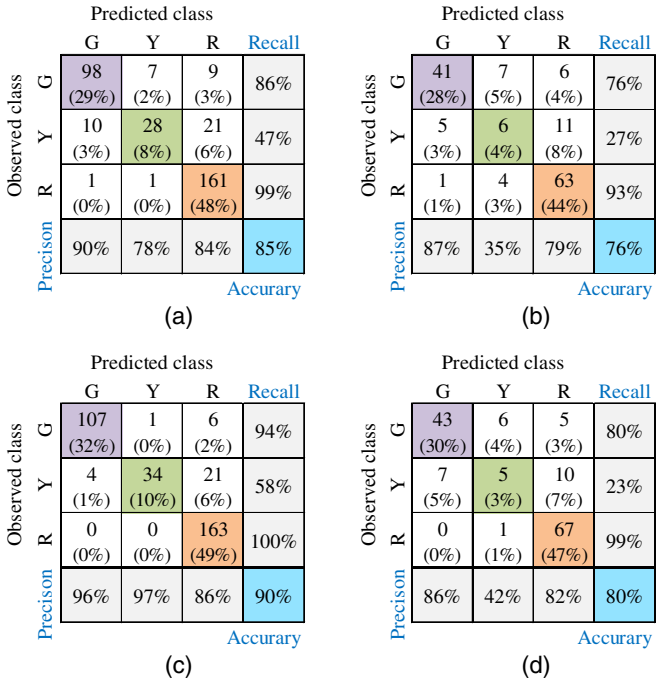

Fig. 13. Confusion matrix for bridge damage data for pool-based sampling: (a) after 50 iterations (training set); (b) after 50 iterations (test set); (c) after 100 iterations (training set); and (d) after 100 iterations (test set).

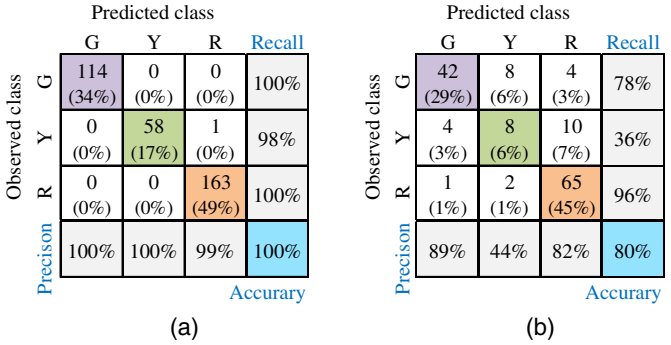

Fig. 14. Confusion matrix for bridge damage state with the entire dataset for (a) training set; and (b) test set.

estimated collectively for the rank-based approach. As shown in Fig. 12, with each query, the accuracies of the training set and the test set increase in pool-based sampling. Detailed performance evaluations of the model with 50 samples, 100 samples, and 480 samples are provided via the confusion matrix, as shown in Figs. 13 and 14. Here, the confusion matrix represents the table of actual tags (obtained from numerical simulations) and predicted tags (from the machine learning model). The precision that is shown in the fourth row represents the relevant predictions, while recall (fourth column) represents the percentage of relevant results correctly predicted through the machine learning model. Note that a good machine learning model should have high precision and high recall for all the tag assessments. The following inferences can be made from the comparison of Fig. 14 (model based on 480 bridge samples) and Fig. 13 (model based on the pool-based sampling strategy with 100 samples):

- The accuracy achieved by the model using 480 samples can be obtained with more efficient sampling approaches.
- Although the accuracies of the models using the entire dataset of 480 samples and 100 pool-based samples are the same, the use of 480 samples (entire dataset) provides higher precision for red, yellow, and green damage states.
- Use of 100 pool-based samples results in higher recall for the red damage state but comes at the cost of low recall and precision for the yellow damage state.
- The accuracy of the training data for 480 data points is higher than that using 100 pool-based samples.
- The precision and recall for the training data of 480 samples are 100%, except recall of the green damage state, while the precision and recall vary with 100 samples.
- Identifying the red damage state is critical for emergency response, and both approaches have fairly good precision and recall for red damage states.

To evaluate the performance of the ranked batch mode sampling approach, samples are queried with a batch size of three, and the XGBoost model, which was built with 10 randomly selected bridge samples, is retrained. The variation of accuracy with query iterations is plotted in Fig. 15, and the confusion matrices for 50

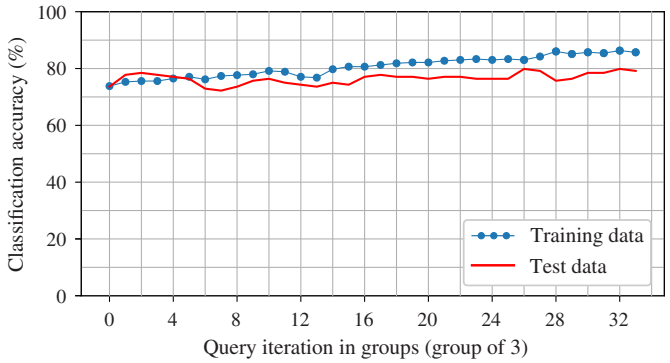

Fig. 15. Incremental classification accuracy for bridge damage state using ranked batch mode sampling.

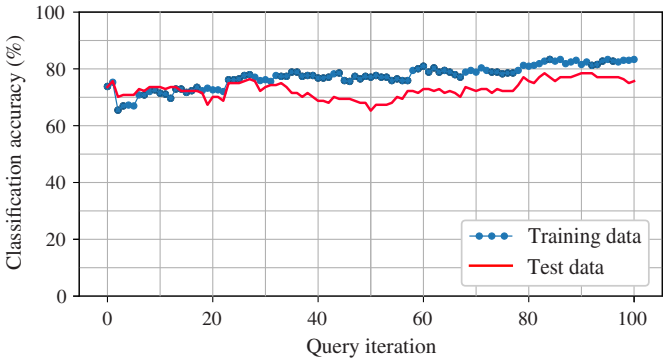

Fig. 17. Incremental classification accuracy for bridge damage state using random sampling.

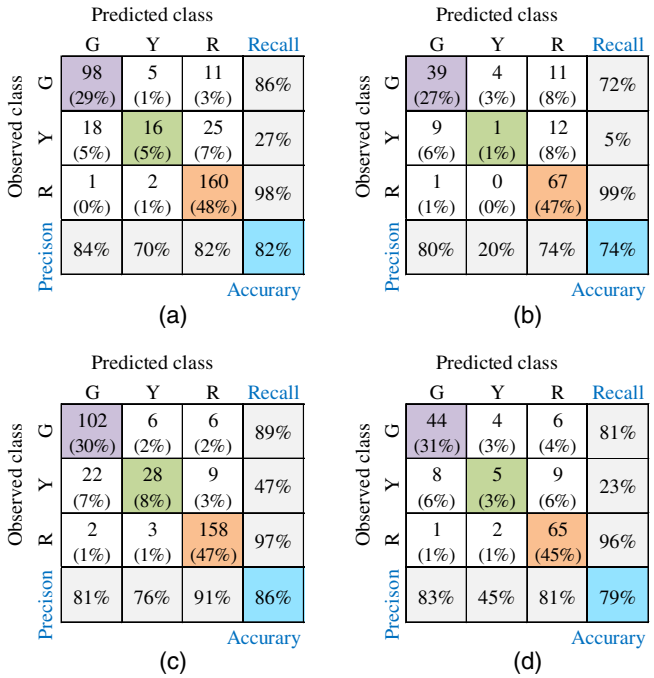

Fig. 16. Confusion matrix for bridge damage state using ranked batch mode sampling: (a) after 50 iterations (training set); (b) after 50 iterations (test set); (c) after 100 iterations (training set); and (d) after 100 iterations (test set).

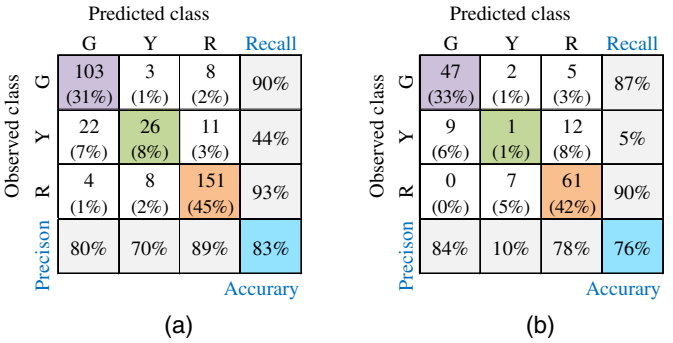

Fig. 18. Confusion matrix for bridge damage state using random sampling: (a) after 100 iterations (training set); and (b) after 100 iterations (test set).

and 100 iterations are provided in Fig. 16. The total accuracy of ranked batch mode sampling is slightly less (<2%) than that of pool-based sampling for the training set for both 50 and 100 iterations.

As expected, the performance of the random learning approach is poor compared to active learning approaches for tagging the bridges. The variation of incremental accuracy with one sample at a time is shown in Fig. 17, where the overall accuracy after 100 iterations is 83% and 76%, respectively, for the training and test set. Also, the confusion matrix of the random sampling after 100 iterations is presented in Fig. 18. As expected, except for the recall of green tag, the precision and recall for other tags are lower in comparison to the pool-based sampling.

A comparison of active learning approaches shows that active learning helps build a machine learning model with fewer samples. In a regional risk assessment scenario, selecting optimal samples for numerical analysis is often difficult, and the proposed approach is a viable alternative. In the two cases, pool-based sampling yields better accuracy compared to ranked batch mode sampling. In the pool-based sampling approach, the samples are queried based on the ones that have the least certainty. Thus, the most informative labels are selected in the pool-based approach, which is the reason for its superior performance in the current study. However, it often comes with a computational expense, as it consists of selecting the sample and doing the numerical or experimental analysis to obtain the output. In an experimental study, the pool-based approach is highly beneficial due to the planning and execution time associated with the experimental studies (e.g., column failure mode). However, in numerical studies (e.g., risk assessment of bridges, here), it is preferable and realistic to run a couple of analyses at a time (for a rapid damage assessment), and thus, batch mode sampling is more meaningful in such scenarios. However, as noted in the current study, it comes with a compromise of the expected accuracy. Therefore, the tradeoff is between the time and accuracy in selecting the best active learning approaches.

Conclusions

Proper seismic regional risk assessment helps to (1) identify critical and vulnerable bridges in a region, and (2) aid emergency responders in planning recovery activities. However, the unique attributes of individual bridges lead to large computational expenses. Although the use of machine learning models is a viable alternative, the accuracy associated with machine learning models is proportional to the data. This paper proposes an approach based on active

learning that can help build machine learning models for damage assessment of bridge systems with a smaller number of informative samples.

To demonstrate the concept of active learning for damage assessment, two research tasks are carried out: (1) failure mode identification of bridge columns, and (2) damage assignment of bridge inventory. Two active learning strategies are used based on how the samples are queried for output: one at a time (pool-based sampling) and in groups (batch mode sampling). In the first task of failure mode identification of bridge columns, the authors use the extensive available experimental database of columns (311 specimens). A model based on 100 samples selected through the pool-based approach achieves 92% relative accuracy (for the training set) with respect to the model based on 311 specimens. Also, the proposed active learning approach is 5% more accurate than the random sampling approach. This observation reveals the potential of active learning in planning experimental studies. To perform the second task, a two-span, single-column seat abutment bridge class in California is used for regional damage assessment. A total of 480 bridge samples are created in this study based on the California bridge inventory and are randomly paired with 480 ground motions for nonlinear dynamic simulations. The demand from each dynamic analysis is compared with the capacity from the associated moment-curvature analysis to determine the damage state of the bridge. As columns are the critical components of bridges, the damage states are classified into (1) green state (no or slight damage), (2) yellow state (yielding of longitudinal rebars and concrete spalling), and (3) red state (irreparable damage). The suggested iterative approach based on active learning with 100 targeted samples can achieve (1) the same accuracy (80%) as one with 480 bridge models, and (2) matching precision and recall in identifying the red damage state, which is critical for emergency response. The creation of such informative models with fewer samples can drastically reduce the computational complexity associated with regional risk assessment.

Although one of the studies uses the experimental database, it is desirable to assess the validity of the active learning model at a regional scale. Currently, the regional risk assessment relies on numerical modeling of bridges for damage assessment, and it is desirable to incorporate real data. Note that the current study is limited to bridge columns and two-bridges in California. The methodology can be further enhanced by adding other bridge types and their associated uncertainties. However, this extension is beyond the scope of the current study. Nonetheless, the proposed active learning approach is applicable to other structures, and further studies are needed in that direction. Through online data-sharing efforts from the earthquake engineering community, the methodology can be further enhanced and examined for other structure types.

Data Availability Statement

Some or all data, models, or code generated or used during the study are available in the GitHub repository: https://github.com/sujithmangalathu/Active_learning_regional_risk_assessment, including the databases of column failure mode and bridge damage state and Python codes of machine learning models.

Acknowledgments

This work was supported by the National Research Foundation of Korea (NRF) grant funded by the Korean government (MSIT) (No. 2020R1A4A1018826).

References

Argyroudis, S. A., S. A. Mitoulis, M. G. Winter, and A. M. Kaynia. 2019. "Fragility of transport assets exposed to multiple hazards: State-of-the-art review toward infrastructural resilience." *Reliab. Eng. Syst. Saf.* 191 (Nov): 106567. https://doi.org/10.1016/j.ress.2019.106567.

Baker, J. W., T. Lin, S. K. Shahi, and N. Jayaram. 2011. *New ground motion selection procedures and selected motions for the PEER transportation research program.* Rep. No. PEER 2011/03. Berkeley, CA: Pacific Earthquake Engineering Research Center, Univ. California.

Cardoso, T. N. C., R. M. Silva, S. Canuto, M. M. Moro, and M. A. Gonçalves. 2017. "Ranked batch-mode active learning." *Inf. Sci.* 379: 313–337. https://doi.org/10.1016/j.ins.2016.10.037.

Chen, T., and C. Guestrin. 2016. "XGBoost: A scalable tree boosting system." In *Proc., 22nd ACM SIGKDD Int. Conf. on Knowledge Discovery and Data Mining*, 785–794. San Francisco: ACM Digital Library. https://doi.org/10.1145/2939672.2939785.

Cohn, D. A., Z. Ghahramani, and M. I. Jordan. 1996. "Active learning with statistical models." *J. Artif. Intell. Res.* 4: 129–145. https://doi.org/10.1613/jair.295.

Dukes, J., S. Mangalathu, J. E. Padgett, and R. DesRoches. 2018. "Development of a bridge-specific fragility methodology to improve the seismic resilience of bridges." *Earthquake Struct.* 15 (3): 253–261. https://doi.org/10.12989/eas.2018.15.3.253.

Friedman, J. H. 2001. "Greedy function approximation: A gradient boosting machine." *Ann. Stat.* 29 (5): 1189–1232. https://doi.org/10.1214/aos/1013203451.

Huang, H., and H. V. Burton. 2019. "Classification of in-plane failure modes for reinforced concrete frames with infills using machine learning." *J. Build. Eng.* 25 (Sep): 100767. https://doi.org/10.1016/j.jobe.2019.100767.

Jeon, J.-S., S. Mangalathu, J. Song, and R. Desroches. 2019. "Parameterized seismic fragility curves for curved multi-frame concrete box-girder bridges using Bayesian parameter estimation." *J. Earthquake Eng.* 23 (6): 954–979. https://doi.org/10.1080/13632469.2017.1342291.

Kiani, J., C. Camp, and S. Pezeshk. 2019. "On the application of machine learning techniques to derive seismic fragility curves." *Comput. Struct.* 218 (Jul): 108–122. https://doi.org/10.1016/j.compstruc.2019.03.004.

Konyushkova, K., R. Sznitman, and P. Fua. 2017. "Learning active learning from data." In *Proc., Advances in Neural Information Processing Systems*, 4225–4235. San Diego: Neural Information Processing Systems Foundation.

Lewis, D. D., and J. Catlett. 1994. "Heterogeneous uncertainty sampling for supervised learning." In *Proc., Machine Learning 1994*, 148–156. Amsterdam, Netherlands: Elsevier.

Mangalathu, S. 2017. "Performance based grouping and fragility analysis of box-girder bridges in California." Ph.D. thesis, School of Civil and Environmental Engineering, Georgia Institute of Technology.

Mangalathu, S., and H. V. Burton. 2019. "Deep learning-based classification of earthquake-impacted buildings using textual damage descriptions." *Int. J. Disaster Risk Reduct.* 36 (May): 101111. https://doi.org/10.1016/j.ijdrr.2019.101111.

Mangalathu, S., G. Heo, and J.-S. Jeon. 2018a. "Artificial neural network based multi-dimensional fragility development of skewed concrete bridge classes." *Eng. Struct.* 162 (May): 166–176. https://doi.org/10.1016/j.engstruct.2018.01.053.

Mangalathu, S., S.-H. Hwang, E. Choi, and J.-S. Jeon. 2019. "Rapid seismic damage evaluation of bridge portfolios using machine learning techniques." *Eng. Struct.* 201 (Dec): 109785. https://doi.org/10.1016/j.engstruct.2019.109785.

Mangalathu, S., H. Jang, S.-H. Hwang, and J.-S. Jeon. 2020. "Data-driven machine-learning-based seismic failure mode identification of reinforced concrete shear walls." *Eng. Struct.* 208 (Apr): 110331. https://doi.org/10.1016/j.engstruct.2020.110331.

Mangalathu, S., and J.-S. Jeon. 2018. "Classification of failure mode and prediction of shear strength for reinforced concrete beam-column joints using machine learning techniques." *Eng. Struct.* 160 (Apr): 85–94. https://doi.org/10.1016/j.engstruct.2018.01.008.

Mangalathu, S., and J.-S. Jeon. 2019a. "Machine learning-based failure mode recognition of circular reinforced concrete bridge columns:

Comparative study." *J. Struct. Eng.* 145 (10): 04019104. https://doi.org/10.1061/(ASCE)ST.1943-541X.0002402.

Mangalathu, S., and J.-S. Jeon. 2019b. "Stripe-based fragility analysis of multispan concrete bridge classes using machine learning techniques." *Earthquake Eng. Struct. Dyn.* 48 (11): 1238–1255. https://doi.org/10.1002/eqe.3183.

Mangalathu, S., J.-S. Jeon, and R. DesRoches. 2018b. "Critical uncertainty parameters influencing seismic performance of bridges using Lasso regression." *Earthquake Eng. Struct. Dyn.* 47 (3): 784–801. https://doi.org/10.1002/eqe.2991.

Mangalathu, S., J.-S. Jeon, J. E. Padgett, and R. DesRoches. 2016. "ANCOVA-based grouping of bridge classes for seismic fragility assessment." *Eng. Struct.* 123 (Sep): 379–394. https://doi.org/10.1016/j.engstruct.2016.05.054.

Mangalathu, S., F. Soleimani, and J.-S. Jeon. 2017. "Bridge classes for regional seismic risk assessment: Improving HAZUS models." *Eng. Struct.* 148 (Oct): 755–766. https://doi.org/10.1016/j.engstruct.2017.07.019.

McKenna, F. 2011. "OpenSees: A framework for earthquake engineering simulation." *Comput. Sci. Eng.* 13 (4): 58–66. https://doi.org/10.1109/MCSE.2011.66.

Morfidis, K., and K. Kostinakis. 2018. "Approaches to the rapid seismic damage prediction of r/c buildings using artificial neural networks." *Eng. Struct.* 165 (Jun): 120–141. https://doi.org/10.1016/j.engstruct.2018.03.028.

Muthukumar, S., and R. DesRoches. 2006. "A Hertz contact model with non-linear damping for pounding simulation." *Earthquake Eng. Struct. Dyn.* 35 (7): 811–828. https://doi.org/10.1002/eqe.557.

Ramanathan, K. N. 2012. "Next generation seismic fragility curves for California bridges incorporating the evolution in seismic design philosophy." Ph.D. thesis, School of Civil and Environmental Engineering, Georgia Institute of Technology.

Seo, J., L. Dueñas-Osorio, J. I. Craig, and B. J. Goodno. 2012. "Metamodel-based regional vulnerability estimate of irregular steel moment-frame structures subjected to earthquake events." *Eng. Struct.* 45 (Dec): 585–597. https://doi.org/10.1016/j.engstruct.2012.07.003.

Seo, J., and D. G. Linzell. 2013. "Use of response surface metamodels to generate system level fragilities for existing curved steel bridges." *Eng. Struct.* 52 (Jul): 642–653. https://doi.org/10.1016/j.engstruct.2013.03.023.

Settles, B. 2010. *Active learning literature survey.* Computer Sciences Technical Rep. No. 1648. Madison, WI: Univ. of Wisconsin–Madison.

Shamsabadi, A., P. Khalili-Tehrani, J. P. Stewart, and E. Taciroglu. 2010. "Validated simulation models for lateral response of bridge abutments with typical backfills." *J. Bridge Eng.* 15 (3): 302–311. https://doi.org/10.1061/(ASCE)BE.1943-5592.0000058.

Shekhar, S., and J. Ghosh. 2020. "A metamodeling based seismic life-cycle cost assessment framework for highway bridge structures." *Reliab. Eng. Syst. Saf.* 195 (Mar): 106724. https://doi.org/10.1016/j.ress.2019.106724.

Siam, A., M. Ezzeldin, and W. El-Dakhakhni. 2019. "Machine learning algorithms for structural performance classifications and predictions: Application to reinforced masonry shear walls." *Structures* 22 (Dec): 252–265. https://doi.org/10.1016/j.istruc.2019.06.017.

Silva, P. F., S. Megally, and F. Seible. 2009. "Seismic performance of sacrificial exterior shear keys in bridge abutments." *Earthquake Spectra* 25 (3): 643–664. https://doi.org/10.1193/1.3155405.

Silva, V., H. Crowley, M. Pagani, D. Monelli, and R. Pinho. 2014. "Development of the OpenQuake engine, the global earthquake model's open-source software for seismic risk assessment." *Nat. Hazards* 72 (3): 1409–1427. https://doi.org/10.1007/s11069-013-0618-x.

Stein, M. 1987. "Large sample properties of simulations using Latin hypercube sampling." *Technometrics* 29 (2): 143–151. https://doi.org/10.1080/00401706.1987.10488205.